nature neuroscience

Long-term dynamics of CA1 hippocampal place codes

Yaniv Ziv[1,5], Laurie D Burns[1,5], Eric D Cocker[1], Elizabeth O Hamel[1], Kunal K Ghosh[2], Lacey J Kitch[1], Abbas El Gamal[2] & Mark J Schnitzer[1,3,4]

Using Ca^{2+} imaging in freely behaving mice that repeatedly explored a familiar environment, we tracked thousands of CA1 pyramidal cells' place fields over weeks. Place coding was dynamic, as each day the ensemble representation of this environment involved a unique subset of cells. However, cells in the ~15–25% overlap between any two of these subsets retained the same place fields, which sufficed to preserve an accurate spatial representation across weeks.

CA1 place cells are considered crucial for spatial memory, but data are limited regarding whether their representations of space evolve over timescales of weeks or more[1]. Some theories suggest place cells should retain stable place fields for long-term retention of familiar environments[1]. Alternatively, dynamic aspects of place coding may facilitate distinct memory traces of different events occurring in the same environment[2]. Studies of modest numbers of cells recorded electrically over, at most, a week[3–9] have found cells with stable place fields, but the data were too sparse to assess how coding evolves at the ensemble level.

We used a viral vector (AAV2/5-CaMKIIα-GCaMP3) to express the Ca^{2+}-indicator GCaMP3 (ref. 10) in pyramidal cells, a preparation for time-lapse imaging of CA1 over weeks[11] and a miniaturized (<2 g) microscope for Ca^{2+} imaging in freely behaving mice[12] (**Fig. 1a**). We thereby tracked somatic Ca^{2+} dynamics of 515–1,040 pyramidal cells per mouse on repeated visits to a familiar track over 45 d.

We first verified CA1 cells' place coding attributes as mice explored various arenas. We saw 73–740 cells, (n = 13 mice) undergoing Ca^{2+} excitation in single fields of view (**Fig. 1b–d**, **Supplementary Fig. 1** and **Supplementary Movie 1**). Ca^{2+} dynamics generally displayed quiescent periods interrupted by prominent transients. This fits with *in vitro* studies showing GCaMP3 reports spike bursts well, but, for solitary spikes, yields weak signals easily masked by background fluorescence or noise[11]. We computationally extracted[13] individual cells and their dynamics from each session's Ca^{2+}-imaging data, without regard to mouse behavior (Online Methods).

As expected of place cells, many pyramidal cells exhibited Ca^{2+} excitation when the mouse explored a specific portion of its arena (**Fig. 1d**). When we placed mice in two different arenas at the same location in the room, but with distinct shape, color and orientation cues, a subset of cells re-mapped[2], showing spatially distinct patterns of Ca^{2+} excitation in the two arenas. As in prior work, some cells had place fields in only one arena. Thus, one can optically detect CA1 place cell activity in freely behaving mice, consistent with a Ca^{2+}-imaging study in mice exploring a virtual reality[14].

To study place cells over weeks, we trained mice to run back and forth on a linear track; Ca^{2+} imaging occurred on ten sessions over 45 d (**Fig. 2a**). As in prior studies in linear environments[15], many cells had clear

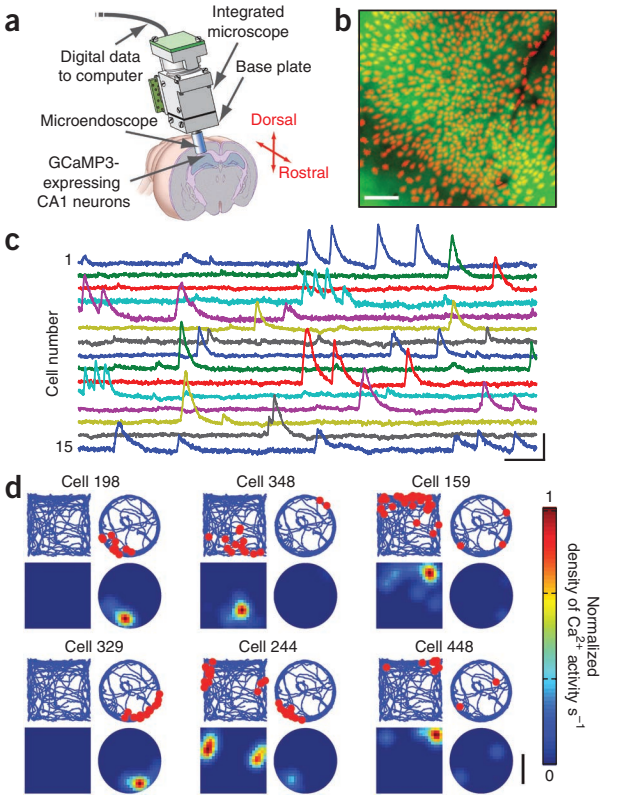

Figure 1 Ca^{2+} imaging in freely behaving mice. (**a**) A tiny microscope equipped with a microendoscope images cells expressing GCaMP3. The microscope's base is fixed to the skull, for repeated imaging of the same cells. (**b**) Shown are 705 cells (red) identified by Ca^{2+} imaging in a behaving mouse, atop a mean fluorescence image (green) of CA1. Blood vessels appear as shadows. (**c**) Relative fluorescence changes ($\Delta F/F$) for 15 cells. (**d**) Spatial distributions of the mouse's location during Ca^{2+} excitation for six example cells in a mouse that explored two arenas. Top panels, blue lines show the mouse's trajectory and red dots mark its position during Ca^{2+} events. Bottom panels, Gaussian-smoothed (σ = 3.5 cm) density maps of Ca^{2+} events, normalized by the mouse's occupancy time per unit area and the cell's maximum response in the two arenas. Scale bars: 100 μm (**b**), 10 s (horizontal) and 5% $\Delta F/F$ (vertical) (**c**), and 20 cm (**d**).

[1]James H. Clark Center, Stanford University, Stanford, California, USA. [2]David Packard Electrical Engineering Building, Stanford University, Stanford, California, USA. [3]Howard Hughes Medical Institute, Stanford University, Stanford, California, USA. [4]CNC Program, Stanford University, Stanford, California, USA. [5]These authors contributed equally to this work. Correspondence should be addressed to M.J.S. (mschnitz@stanford.edu) or Y.Z. (yziv@stanford.edu).

Received 29 October 2012; accepted 9 January 2013; published online 10 February 2013; corrected online 11 February 2013 (details online); doi:10.1038/nn.3329

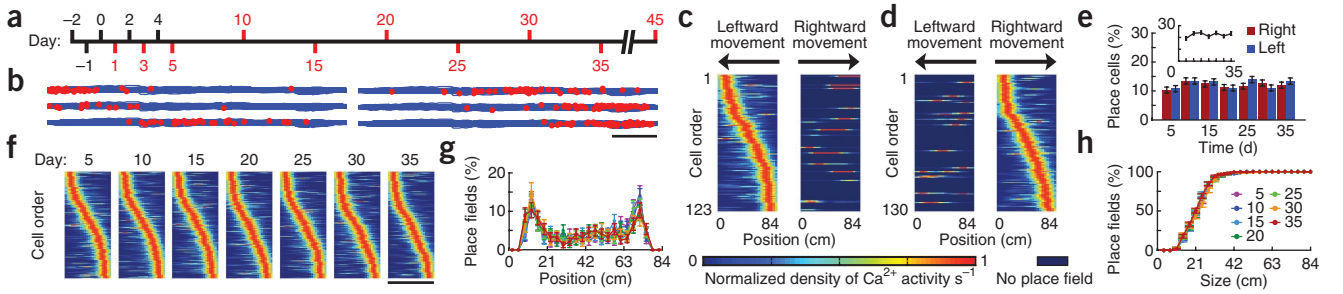

Figure 2 Basic aspects of CA1 place codes are stable for weeks. (**a**) Black, training days; red, imaging. (**b**) The mouse's trajectory (blue lines) and its locations during cellular Ca^{2+} excitation (red dots) illustrate place cell activity. (**c**,**d**) Gaussian-smoothed (σ = 8.75 cm) maps of Ca^{2+} activity on the track, for the subsets of cells on day 15 with significant place fields during left (**c**) or right (**d**) motion. Dark blue marks the lack of a place field for one of the two directions. Cells from four mice were pooled, ordered by place fields' centroid locations. Ca^{2+} maps were normalized by each cell's maximum activity during left (**c**) and right (**d**) motion. (**e**) Fraction of cells with significant place fields, expressed as a percentage of cells found in each session (807–1,000 total cells per day, n = 4 mice), for each motion direction (bars) and in total (inset). (**f**) Place fields for each session, displayed as in **c** and **d**, ordered by centroid location on each day and pooled across four mice and both motion directions. (**g**) Spatial distributions of place fields' centroid locations (3.5-cm bins, n = 4 mice, 178–268 cells per day). Color key is shown in **h** and indicates day of imaging. (**h**) Cumulative distributions of place fields' widths; median (±33% confidence interval), 24 ± 3.5 cm. Scale bars: 10 cm (**b**) and 84 cm (**f**). Error bars, s.e.m.

place-coding properties that usually depended strongly on the mouse's running direction (**Fig. 2b–d**). For detailed analyses, we focused on four mice and used a conservative definition of place field by requiring statistically significant mutual information between a cell's Ca^{2+} excitation events and the mouse's location[16]. With this definition, ~20% of cells had place fields for left, right or both directions (**Fig. 2c–e**). The set of place fields fully covered the track, with the ends covered more densely than the interior (**Fig. 2f,g**). The mean place field size was ~27% of the 84-cm track, in the range for mice[14,15,17,18]. For each place field, we detected Ca^{2+} activity in 17 ± 14% of passes (n = 1,656 place fields, mean ± s.d., range = 2–87%). Across days 5–35, the percentages of cells on each day with place fields for right (12 ± 1%, mean ± s.e.m.) or left (12 ± 1%) motion did not vary (n = 7 sessions, 4 mice, Kruskal-Wallis ANOVA, P = 0.77 for right, 0.88 for left; **Fig. 2e**). Nor were there changes in the distributions of place fields' locations or sizes (Kolmogorov-Smirnov test, P = 0.06–0.99 for locations and 0.02–0.99 for sizes, both compared with a significance threshold of 2.4×10^{-3} that includes the Dunn-Sidák correction for the 21 pairwise comparisons; **Fig. 2g,h**). We saw no discernible changes to cells' morphologies or substantial changes in mean Ca^{2+}-transient amplitudes or baseline fluorescence within or across sessions (**Supplementary Fig. 2**). Thus, photobleaching was negligible, and neither GCaMP3 expression nor illumination had perceptibly deleterious effects on cell health.

For cells seen on multiple days, bootstrap analysis showed that errors in aligning cells' locations across sessions were <1 µm (**Supplementary Fig. 3**). This precision more than sufficed, as even the closest cells had ≥6 µm between centroids. Each mouse yielded 515–1,040 cells total (n = 4 mice), more than the maximum (740) seen in one session, but consistent with anatomical data.

A majority of cells was active in one or two sessions (57 ± 1%, mean ± s.d., n = 2,960 cells, 4 mice); 2.8 ± 0.3% were active in all ten sessions (**Fig. 3a,b**). However, each session had the same percentage (31 ± 1%) of active cells out of the full tally (Kruskal-Wallis ANOVA, P = 0.46; **Fig. 3b**). Cells came in and out of this active subset, but the overlap in active subsets from any two days was only moderately time dependent: ~60% for sessions 5 d apart, ~40% for 30 d apart (**Fig. 3c**).

Between any two sessions, there was ~15–25% overlap in the subsets of cells with statistically significant place fields, declining from ~25% for sessions 5 d apart to ~15% for 30 d (**Fig. 3c**). Notably, when individual cells did show place fields in more than one session, the place fields' locations were generally identical (**Fig. 3d**). This is an independent validation of our image registration protocol. Although cells came in and out of the place-coding ensemble, place fields' invariant locations, along with the slowly declining overlap in place-coding ensembles, led to spatial representations that retained a clear resemblance while decaying over time (**Fig. 3e–g**).

We next sought factors that influenced cells' recurrences in the place-coding ensemble. If cell physiological or coding parameters are key, Ca^{2+} activity or place-coding parameters might correlate with recurrence probabilities. If network dynamics are more important, the data might reveal no relationships between cells' characteristics and recurrence probabilities. Notably, the numbers of sessions in which cells had Ca^{2+} activity or place fields were uncorrelated with their rates and amplitudes of Ca^{2+} activation (**Supplementary Fig. 4**). Cells with high place-coding stability in single sessions had virtually the same recurrence odds as other cells (**Supplementary Fig. 5**). Neither inclusion of Ca^{2+} transient amplitudes in the computations of place fields nor variations in how we extracted cells from the raw data altered these findings (**Supplementary Figs. 6** and **7**).

Given place fields' invariant locations, did the ~15–25% overlap between different days' coding ensembles suffice to retain a stable spatial representation? We used Bayesian decoding to study how well we could reconstruct the mouse's location from the Ca^{2+}-imaging data (**Fig. 3h–j** and **Supplementary Fig. 8**). We created a set of decoders of a common mathematical structure, trained each decoder on a portion of one day's data, and tested it on other data. When test and training data were from the same day, estimates of mouse location were excellent (median error nearly always <7 cm) and highly significant compared with shuffled test data ($P < 10^{-160}$, Kolmogorov-Smirnov test). We then asked how well a decoder trained on data recorded on one day would perform on data recorded on other days. In comparisons between decoders using the same number of cells, performance declined only modestly with the interval between training and testing and remained very significant for 30-d intervals ($P = 10^{-27}$, Kolmogorov-Smirnov test). Thus, the ~15% commonality in place-coding subsets across 30 d sufficed to deduce the mouse's trajectory using a decoder trained on data of 30 d prior.

Although GCaMP3 does not faithfully report single spikes[10], our approach can sense isolated spike bursts. To evade analyses of place coding by using only solitary spikes, cells would have to avoid burst spiking across entire sessions while still encoding spatial information. We do not exclude this possibility, but consider it unlikely, given the important place-coding role ascribed to bursts[19] and the observed

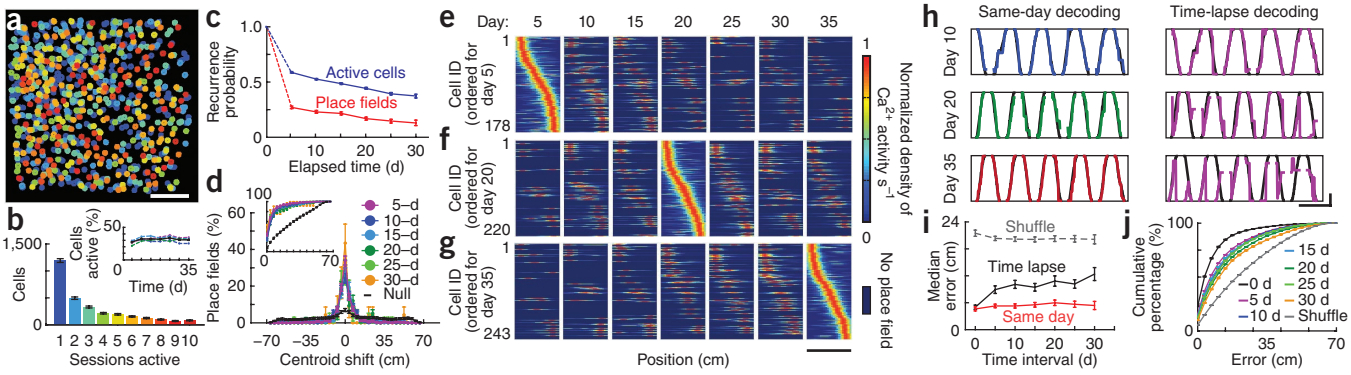

Figure 3 Place fields are spatially invariant and temporally stochastic while preserving a stable representation at the ensemble level. (**a**) We found Ca^{2+} activity in 826 cells in one mouse over 45 d. Color as in **b**. (**b**) Histogram of the number of sessions in which each of 2,960 cells from four mice was active. Error bars, s.d. from counting statistics. Inset, a constant fraction of all cells detected over ten sessions was active each day. Colored data, individual mice; black, mean ± s.e.m. (**c**) If a cell had Ca^{2+} activity in one session, the odds (blue data) that it also did in a subsequent session declined with time. If a cell had a statistically significant place field in one session, the odds (red data) that it had a place field in a subsequent session also declined with time. Mean ± s.e.m. (**d**) Distributions of centroid shifts (colored by days between sessions, mean ± s.e.m.) were indistinguishable (Kolmogorov-Smirnov test, $P \geq 0.17$), sharply peaked at zero and highly distinct from the null hypothesis that place fields would randomly relocate ($P = 4 \times 10^{-67}$, Kolmogorov-Smirnov test). Inset, cumulative histograms of shift magnitudes; 74–83% were ≤7 cm. Median shift (3.5 cm) was much less than the median place field width (24 cm). (**e**–**g**) Place-field maps for cells found on multiple days, ordered by place fields' centroid positions on day 5 (**e**), day 20 (**f**) or day 35 (**g**). Data pooled across four mice. (**h**) Time-lapse decoders retain accuracy over 30 d. Reconstructions of the mouse's trajectory (colored curves) and its actual position (black curves); three paired reconstructions comparing time-lapse decoders trained on data from day 5 (right), using all cells with place fields on both days of each pair, and decoders trained on data from the same day as the test trial (left). Each pair used an equal number of cells, optimally chosen at left to minimize errors. (**i**) Median errors in estimating the mouse's position were ~7–13 cm, even for decoders trained on data from 30 d prior (black, mean ± s.e.m.). Red, decoders trained on data from the same day as test data, using equal numbers of cells as black points and optimally chosen to minimize errors. Gray, errors using shuffled traces of Ca^{2+} activity from the same day as training data (averaged over 10,000 shuffles). (**j**) Cumulative distributions of decoding error magnitudes (mean ± s.e.m.) for test and training data separated by the indicated times or (gray) for decoders tested on shuffled data. Scale bars: 100 μm (**a**), 84 cm (**e**–**g**), and 2 s (horizontal) and 10 cm (vertical) (**h**).

lack of correlation between cellular Ca^{2+} activity and involvement in place coding. Improved Ca^{2+} sensors should reveal a greater portion of spiking activity and could amend our findings with GCaMP3.

Our data indicate that retention of spatial information in CA1 combines stable place field locations with ~15–25% odds an individual cell will recur in the place code. Prior long-term recordings had stressed place-field stability and usually focused on tens of cells or fewer. By reliably tracking ~3,500 CA1 cells over weeks[11], we found that place-coding ensembles have a fluctuating membership. This supports prior reports of individually stable place fields, but shows CA1 coding has day-to-day dynamism at the cellular level while preserving spatial information in the ~15–25% overlap between coding ensembles from any two days. Conversely, each episode in a familiar arena has a unique signature via the ~75–85% of cells that do not overlap in coding ensembles from any two sessions (**Fig. 3c**). It is possible that coding turnover is a long-term form of the spike-rate re-mapping seen over shorter intervals[2]. Such a coding scheme might aid episodic memory by creating distinct traces for events occurring in the same environment but at different times.

METHODS

Methods and any associated references are available in the online version of the paper.

Note: Supplementary information is available in the online version of the paper.

ACKNOWLEDGMENTS

We thank L. Looger (Janelia Farm Research Campus) for GCaMP3 plasmid, and A. Attardo, T. Davidson, J. Fitzgerald, J. Li, J.Z. Li, A. Lui, C. Ramachandran, O. Yizhar and T. Zhang for conversations and assistance. We appreciate fellowships from the US National Science Foundation (L.D.B., L.J.K.), the Simons (L.J.K.) and Machiah (Y.Z.) Foundations and research funding to M.J.S. from the Paul G. Allen Family Foundation and the US National Institutes of Health (grants DP1OD003560, R21AG038771 and R21MH099469).

AUTHOR CONTRIBUTIONS

Y.Z., L.D.B. and M.J.S. designed experiments. Y.Z., L.D.B. and E.O.H. acquired data. L.D.B. and L.J.K. analyzed data. L.D.B., E.D.C. and K.K.G. built equipment. Y.Z., L.D.B., L.J.K. and M.J.S. wrote the paper. A.E.G. and M.J.S. supervised.

COMPETING FINANCIAL INTERESTS

The authors declare competing financial interests: details accompany the online version of the paper.

Published online at http://www.nature.com/doifinder/10.1038/nn.3329.
Reprints and permissions information is available online at http://www.nature.com/reprints/index.html.

1. O'Keefe, J.N.L. *The Hippocampus as a Cognitive Map* (Clarendon, 1978).
2. Leutgeb, S. *et al. Science* **309**, 619–623 (2005).
3. Muller, R.U., Kubie, J.L. & Ranck, J.B. Jr. *J. Neurosci.* **7**, 1935–1950 (1987).
4. Thompson, L.T. & Best, P.J. *Brain. Res.* **509**, 299–308 (1990).
5. Kentros, C. *et al. Science* **280**, 2121–2126 (1998).
6. Lever, C., Wills, T., Cacucci, F., Burgess, N. & O'Keefe, J. *Nature* **416**, 90–94 (2002).
7. Kentros, C.G., Agnihotri, N.T., Streater, S., Hawkins, R.D. & Kandel, E.R. *Neuron* **42**, 283–295 (2004).
8. Cacucci, F., Wills, T.J., Lever, C., Giese, K.P. & O'Keefe, J. *J. Neurosci.* **27**, 7854–7859 (2007).
9. Muzzio, I.A. *et al. PLoS Biol.* **7**, e1000140 (2009).
10. Tian, L. *et al. Nat. Methods* **6**, 875–881 (2009).
11. Barretto, R.P. *et al. Nat. Med.* **17**, 223–228 (2011).
12. Ghosh, K.K. *et al. Nat. Methods* **8**, 871–878 (2011).
13. Mukamel, E.A., Nimmerjahn, A. & Schnitzer, M.J. *Neuron* **63**, 747–760 (2009).
14. Dombeck, D.A., Harvey, C.D., Tian, L., Looger, L.L. & Tank, D.W. *Nat. Neurosci.* **13**, 1433–1440 (2010).
15. McHugh, T.J., Blum, K.I., Tsien, J.Z., Tonegawa, S. & Wilson, M.A. *Cell* **87**, 1339–1349 (1996).
16. Markus, E.J., Barnes, C.A., McNaughton, B.L., Gladden, V.L. & Skaggs, W.E. *Hippocampus* **4**, 410–421 (1994).
17. Nakazawa, K. *et al. Neuron* **38**, 305–315 (2003).
18. Rotenberg, A., Mayford, M., Hawkins, R.D., Kandel, E.R. & Muller, R.U. *Cell* **87**, 1351–1361 (1996).
19. Lisman, J.E. *Trends Neurosci.* **20**, 38–43 (1997).

ONLINE METHODS

Viral vector. University of North Carolina Vector Core packaged AAV2/5 vectors (~2×10^{12} particles per ml) expressing GCaMP3 via the *Camk2a* promoter[20]. We used immuno-staining of virally infected CA1 tissue to verify GCaMP3 and CaMKII co-expression in the same cells.

Mice. Stanford APLAC approved all procedures. Male C57BL/6 mice (aged 8–12 weeks at start, housed 2–3 per cage with a running wheel) underwent two procedures under isoflurane (1.5–2%, vol/vol). We first injected AAV2/5-CaMKIIα-GCaMP3 (refs. 10,14) (250 nl) into CA1 (–1.9 mm from Bregma, 1.4 mm mediolateral, –1.65 mm dorsoventral). A week after viral transduction we implanted a glass guide tube just dorsal to CA1, as described previously[11].

Ca^{2+} imaging. We used the integrated microscope as described for imaging CA1 (ref. 12), with minor adaptations for time-lapse studies[11,21]. The first session (~4 weeks after second surgery) began by installing the microendoscope into the guide tube of isoflurane-anesthetized mice, guided by two-photon imaging of CA1 through the microendoscope[11,21,22]. The microendoscope was a gradient refractive index lens (GRINtech GmbH, 0.44 pitch length, 0.47 NA) and relayed light from CA1 to a focal plane outside the mouse. After verifying GCaMP3 expression, we fixed the microendoscope in the tube using ultraviolet-curing adhesive (Norland, NOA 81).

We lowered the integrated microscope toward the microendoscope until we saw GCaMP3 fluorescence using the microscope's LED light source (0.05–0.2 mW). After finding a suitable imaging site, we attached to the cranium the microscope's base plate using dental acrylic and Cerebond. This plate stayed with the mouse even when the microscope was detached. We generally darkened the acrylic with carbon powder (Sigma, 484164).

Mice displayed vigorous activity ~1–2 min after release from anesthesia. We chose isoflurane for its rapid clearance from tissue, but nevertheless waited 20–30 min before imaging. Illumination (<0.4 mW) lasted ~3 min per imaging trial. Each session on the track involved 4–7 trials, over which the mouse usually ran >50 roundtrip passes. During ~3 min between trials, the mouse rested in a holding chamber. After all trials, we waited another 10–15 min, then briefly (~5 min) re-anesthetized the mouse to detach the microscope. A typical session yielded <25 min of video (19.9 Hz, 480 × 480 pixels covering ~0.34 mm^2 of CA1).

In the following sessions, we re-attached the microscope to its base while the mouse was isoflurane anesthetized (~5 min), then waited 20–30 min before imaging. We verified the field of view matched prior sessions or made slight focal adjustments[12]. Subsequent steps were as described above.

Behavioral analysis. During Ca^{2+} imaging the mouse explored a square 46 × 46 × 15 cm^3 arena (acrylic), a circular arena (21-cm radius, red plastic) or an 84 × 4.5 × 4.5 cm^3 elevated linear track (aluminum). For 3 d prior to Ca^{2+} imaging on this track, we trained water-scheduled mice to run back and forth for water rewards at the ends. An overhead camera (Prosilica, EC640) recorded this behavior using infrared LEDs (Lorex, VQ2120) and dim room lights for illumination.

We analyzed videos using MATLAB (Mathworks) and set all pixels to zero or one if their intensities were, respectively, above or below 10% of the median intensity. This demarcated the mouse because of its dark fur. We determined the mouse's position as the centroid of each binary image and calculated its velocity after smoothing the position data (0.5-s sliding average).

Basic processing of Ca^{2+}-imaging videos. Analysis used ImageJ (US National Institutes of Health) and MATLAB routines. Because the microscope's sensor had a Bayer color filter[12], we zeroed all pixels in the red and blue channels and demosaiced GCaMP3 signals in the green pixels by Bayer interpolation using the MATLAB function demosaic(). Image rows were read out successively; to correct for the slightly variable number of LED pulses illuminating each row, we normalized each demosaiced pixel by the mean intensity in its row. The illumination exhibited mild spatial non-uniformity, so we also normalized each pixel by the ratio of the mean intensity along its column to that of a reference column. We coarse-grained images to 240 × 240 pixels, each of which was the mean of four pixels at the finer density.

We used rigid image registration to correct lateral displacements of the brain. We created an image stack, $F_2(t)$, as the difference between the original stack, $F(t)$, and a smoothed version of $F(t)$ (20-pixel-radius smoothing filter). Within $F_2(t)$, we selected a high-contrast subregion to provide a fiducial marker. To mutually register all frames of $F_2(t)$, we used an ImageJ plug-in based on the TurboReg algorithm[23]. For each registered frame of $F_2(t)$, we applied the same coordinate transformation to $F(t)$, yielding the registered stack $F'(t)$.

Identification of neurons. As is typical for Ca^{2+} imaging, we re-expressed registered images as relative changes in fluorescence, $\Delta F'(t)/F'_0 = (F'(t) - F'_0)/F'_0$, where F'_0 is the mean image obtained by averaging the entire movie. We identified spatial filters corresponding to individual cells using an established cell-sorting algorithm that applies principal and independent component analyses[12,13,24]. Cells' spatial filters were based on Ca^{2+} activity (temporally down-sampled 4×) over the entire session, not just when the mouse was running. For each filter, we zeroed all pixels with values <50% of that filter's maximum intensity.

Detection of Ca^{2+} transients. We used each cell's thresholded spatial filter to extract its Ca^{2+} activity from the $\Delta F'(t)/F'_0$ stack. We removed baseline fluctuations (ascribed to Ca^{2+} activity outside the focal plane or in neuropil) by subtracting the median trace (200 time bins sliding window) and applied a 5 frame (~250 ms) sliding average. We identified Ca^{2+} transients by searching each trace for local maxima that had peak amplitude more than two s.d. (2σ) from the trace's baseline, ≥10 frames (~0.5 s) when the mean intensity surrounding the peak was >2σ, and separation of >6 frames (~300 ms) from adjacent Ca^{2+} transients. We set a Ca^{2+} transient's occurrence to the temporal midpoint in the rise to peak fluorescence from the most recent trough, approximating a time midway in the corresponding spike burst. To correlate Ca^{2+} activity to mouse behavior, we offset Ca^{2+} transient occurrences by ~250 ms because of GCaMP3's known delayed response[10].

On ~7% of all detected Ca^{2+} transients, fluorescence increases occupied more pixels than a single spatial filter. To mitigate the effects of this spillover, we took a conservative approach, allowing only one cell among a group of neighbors to register a Ca^{2+} transient in a ~250-ms window. We defined neighbors as cells whose spatial filters had nonzero pixels within 30 μm of each other. If multiple Ca^{2+} transients arose within ~250 ms in neighboring cells, we retained only the transient with the greatest peak $\Delta F'(t)/F'_0$ value.

Registration of cells across sessions. We mapped all cells from each session by assembling their thresholded spatial filters onto a single image. Picking one day's map for reference (usually day 15), we aligned the others to this via a scaled image alignment using TurboReg[23] (**Supplementary Fig. 3a**). This corrected slight translations, rotations or focus-dependent magnification changes between sessions and yielded each cell's location in the reference coordinate system.

Next, we visually identified candidate cells across sessions that might be the same neuron seen on multiple occasions. We applied two observations: our registration procedures had submicron precision (**Supplementary Fig. 3b–e**) and the distance between centroids of neighboring somata was always >6 μm (**Supplementary Fig. 3f**). We therefore considered a candidate set of cells to be the same neuron if all pairwise separations were ≤6 μm. If any of the pairwise separations exceeded 6 μm, we split the set into two or more.

Place fields. To analyze place fields, we identified movement periods when the mouse ran continuously >0.5 cm s^{-1}. In addition, in open field arenas the speed had to exceed 1 cm s^{-1} at some point during the movement; on the track it had to transiently exceed 9.2 cm s^{-1}. These criteria rejected small movements such as grooming, rearing or head turning.

On the linear track, we considered 3.5-cm spatial bins and excluded the last 7 cm at each end where water rewards were given. In open field arenas, bins were 4 cm^2. We divided the number of Ca^{2+} transients in each bin by the mouse's total occupancy time there, applied a Gaussian smoothing filter (linear track, σ = 8.75 cm; open field, σ = 3.5 cm), and normalized each place field by its maximum value. On the track, we separately considered place fields for left and right running directions. The number of bins in which a place field had a value ≥50% of its maximum determined the place field's width. We tabulated each place field's position as its centroid.

Statistical analysis. For each place field (calculated for one running direction), we computed the mutual information[25] between Ca^{2+} transients and the mouse's location (7-cm bins). We also performed 10,000 distinct shuffles of the Ca^{2+} transient

times and calculated the mutual information for each shuffle. This yielded the *P* value of the true mutual information relative to the shuffles. $P \leq 0.05$ indicated a significant place field for that running direction.

To generate the null hypothesis for place fields' displacements between a pair of days, we used the place fields' measured locations, but shuffled cells' identities on each of the days. We calculated the distribution of all displacements, averaged over 1,000 distinct pairs of shuffles. **Figure 3d** shows the mean null hypothesis curve found by averaging over all pairs of days.

Decoding. We used Bayesian methods[26,27] to estimate mouse location based on cells' Ca^{2+} transients (**Supplementary Fig. 8**).

20. Gradinaru, V. *et al. J. Neurosci.* **27**, 14231–14238 (2007).
21. Barretto, R.P., Messerschmidt, B. & Schnitzer, M.J. *Nat. Methods* **6**, 511–512 (2009).
22. Barretto, R.P.J. & Schnitzer, M.J. in *Imaging: a Laboratory Manual* (ed. R. Yuste) Ch. 50 (Cold Spring Harbor Laboratory Press, 2011).
23. Thévenaz, P., Ruttimann, U.E. & Unser, M. *IEEE Trans. Image Process.* **7**, 27–41 (1998).
24. Nimmerjahn, A., Mukamel, E.A. & Schnitzer, M.J. *Neuron* **62**, 400–412 (2009).
25. Shannon, C.E. & Weaver, W. *The Mathematical Theory of Communication* (University of Illinois Press, 1949).
26. Brown, E.N., Frank, L.M., Tang, D., Quirk, M.C. & Wilson, M.A. *J. Neurosci.* **18**, 7411–7425 (1998).
27. Quian Quiroga, R. & Panzeri, S. *Nat. Rev. Neurosci.* **10**, 173–185 (2009).

doi:10.1038/nn.3329